Controller Performance Evaluation of Fly-by-Feel (FBF) Technology

Project WBS Number: WBS: 694478.02.93.02.11.05.24

Investigator(s): Marty Brenner (NASA DFRC), Arun Mangalam (Tao Systems)

Background

Fly-by-feel (FBF) is a new paradigm for safely maximizing aircraft stability and performance across a wide range of conditions wherein the aircraft autonomously and intelligently senses the aerodynamic environment and efficiently adapts the aircraft structure and control surfaces to suit the current mission objectives. FBF depends on an integrated active approach to flight control, structural mode attenuation, and flow control. Desired flight performance, gust load alleviation and aerostructural stability in the presence of complex aeroservoelastic (ASE) model uncertainties are met by utilizing aerodynamic observables in a robust control law framework.

As opposed to conventional systems, flow bifurcation point sensors will be used as aerodynamic observables to estimate, in real-time without the delay of structural response, aerodynamic coefficients, which in turn will be used as direct aerodynamic force feedback for flight control resulting in minimization of ASE uncertainties. Sensors are integrated in a physics-based architecture that improves reliability, control effectiveness and robustness through a spatially distributed network, and this effort is a first step in showing feasibility. This wind tunnel test effort and data analysis provides for the first time a validation of the closed-loop control using aerodynamic observables for force feedback through flow bifurcation points. The resulting architecture will be scalable to flight.

The National Aeronautics R&D Plan describes concepts that could be separated into two parts: (1) monitoring technology: structurally integrated sensors, distributed sensing systems, physics-based transition prediction, and aircraft-level health-management; and (2) control technology: actively controlled wing structures, novel flow control techniques, and advanced flight controls for aircraft efficiency. The proposed system, once validated, will help satisfy the above needs with a physics-based embedded sensor architecture distributed across the wing span.

This research activity provides a foundation for FBF-based control of sub/tran/supersonic aircraft, including UAVs and long-endurance platforms, using aerodynamic observables with distributed control methodologies. Demonstration of a precedent system has shown potential on an AFRL SensorCraft configuration in the NASA Langley Transonic Dynamics Tunnel. This effort will provide the basis for transitioning the architecture to platforms such AFRL/LM Multi-utility Aeroelastic Demonstrator / Test Technology (MAD-MUTT) aircraft and NASA F18-FAST flight tests.

Approach

The primary objective is to provide a technical basis for determining the extent of performance improvement of the FBF approach under operational flight conditions in comparison to conventional flight control systems. Secondary objectives include: (1) determining the relationship between aerodynamic observables with aeroelastic instabilities, loads/moments and control surface actuation in a nonlinear free pitch-and-plunge apparatus (PAPA) for a representative wing; (2) validating computational models predicting the aerodynamic coefficients (CL, CM and CD) based on pitch/plunge/actuator state and aerodynamic observables; (3) determining the accuracy/robustness of system identification techniques in capturing the nonlinear system parameters; and, (4) characterizing the performance of conventional and robust control laws using a variety of output for feedback including aerodynamic observables in unsteady flow.

To provide a basis for the next phase of the program, we (1) use a representative 2D wing with control surfaces instrumented with flow sensors, accelerometers and a load cell; (2) model the dynamic interactions and uncertainties in aerodynamics, structures, sensing and actuation, e.g., freeplay; (3) develop and implement robust system identification techniques to capture the nonlinear parameters of the system; (4) design and simulate robust control laws augmented with the aerodynamic observables; (5) conduct open-loop/closed-loop wind tunnel tests in a free PAPA to validate the computational (unsteady) results; and, (6) conduct a post-test analysis of the conventional and FBF system identification and control performance.

Accomplishments

The primary Phase 1 objective is to provide a technical basis for determining the extent of performance improvement of the FBF approach under operational flight conditions in comparison to conventional flight control systems. Our secondary objectives include: (1) determining the relationship between aerodynamic observables with

aeroelastic instabilities, loads/moments and control surface actuation in a nonlinear free pitch-and-plunge apparatus (PAPA) for a representative wing, (2) validating computational models predicting the aerodynamic coefficients (CL, CM & CD) based on pitch / plunge / actuator state and aerodynamic observables, (3) determining the accuracy/robustness of system identification techniques in capturing the nonlinear system parameters, and (4) characterizing the performance of control laws using a variety of output for feedback including aerodynamic observables.

To achieve these objectives, a wing with active control surfaces has been calibrated in the free PAPA at Texas A&M University (TAMU) 2-ft $\times$ 3-ft subsonic tunnel. A procedure was developed to test the wing at increasing airspeed to determine the limit cycle oscillation (LCO) margin. In addition, a wing with the same airfoil section as the X-56A vehicle has been instrumented and installed in the TAMU 3-ft $\times$ 4-ft subsonic tunnel. The wing was installed in a forced PAPA, and pitched at frequencies ranging up to 5 Hz. Based on the data, this wing will be calibrated for upcoming ASE flight tests. Both free and forced PAPA tests are useful to determine the effect of unsteadiness on the aerodynamic forces.

With the X-56A wind tunnel model, we conducted tests with over 400 runs, including the following for two airspeeds:

- Pitch dwells and sweeps. If we consider $\alpha(t) = A_\alpha \cos(2\pi f_\alpha(t)t) + \alpha_0$, where α is the pitch angle, A_α is the pitch amplitude, f_α is the pitch frequency and α_0 is the mean pitch angle, then we tested a combination of $A_\alpha = \{2, 5, 10, 20\}$ degrees, $\alpha_0 = \{0, 10\}$ degrees and $f_\alpha = \{0.01, 1, 2, 3, 4, 5\}$ Hz.

- Pitch steps. Pitch steps at mean pitch angles of 0, 5, 10 and 15 degrees with a pitch step amplitude of 5 and 10 degrees. The purpose of the pitch step is to emulate the Wagner function output for modeling unsteady aerodynamics at various mean pitch angles.

- Plunge dwells and sweeps. If we consider $h(t) = A_h \cos(2\pi f_h(t)t) + h_0$, where h is the plunge displacement, A_h is the plunge amplitude, f_h is the plunge frequency and h_0 is the mean plunge displacement, then we tested a combination of $A_h = \{0.5, 1.5\}$ inches, $h_0 = \{0, -3\}$ inches and $f_h = \{1, 2, 3\}$ Hz.

The data includes (1) accelerations from the wing and forced PAPA apparatus, (2) aerodynamic forces and moments as calculated using a load balance, (3) pitch/plunge encoder output, (4) LESP location, and (5) airspeed. The data was recorded at 500 Hz.

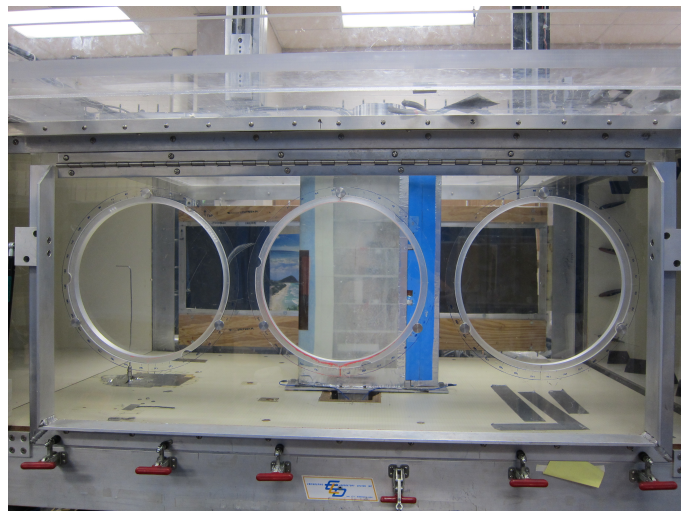

Figure 1: Instrumented wing in TAMU free PAPA

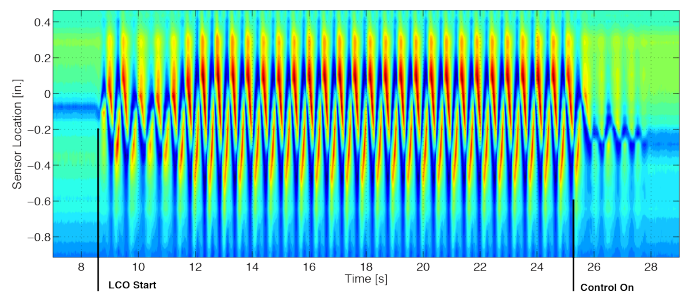

Figure 2: Limit cycle oscillation and control

For the free PAPA test, the free PAPA test section is shown in Figure 1. The figure depicts the airfoil instrumented with surface sensors near the leading-edge to determine the LESP location in real-time. There is also a trailing-edge control surface for actively controlling the wing to suppress the LCOs at higher speeds. Figure 2 depicts the flow sensor output near the leading-edge during an LCO. Figure 2 also shows the control of the LCO using an accelerometer-based controller. Blue represents low relative shear stress and red represents high shear stress. The LESP is clearly visible as the oscillating minimum shear stress.

To develop the LESP-based controller, we must first statically calibrate the LESP sensors with aerodynamic lift. By obtaining aerodynamic lift, we could use the constituent aeroelastic equations to develop an ASE controller to suppress the LCOs. Figure 3 depicts a calibration of LESP output with the loss in lift coefficient. The use of this calibration results in the estimated lift coefficient in Figure 4. The lift coefficient versus angle of attack is shown in Figure 5. We could consequently see that the flow is three-dimensional, since there is a loss in lift from ideal two- dimensional flow. Considering the flow is three-dimensional, the estimation in Figure 5 is

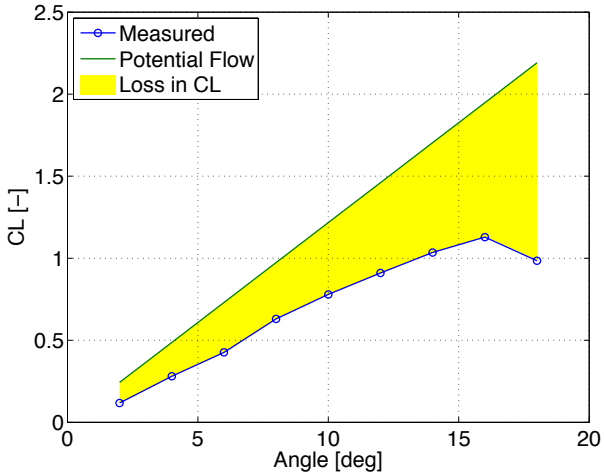

Figure 3: Steady flow calibration of LESP with loss-in-lift coefficient

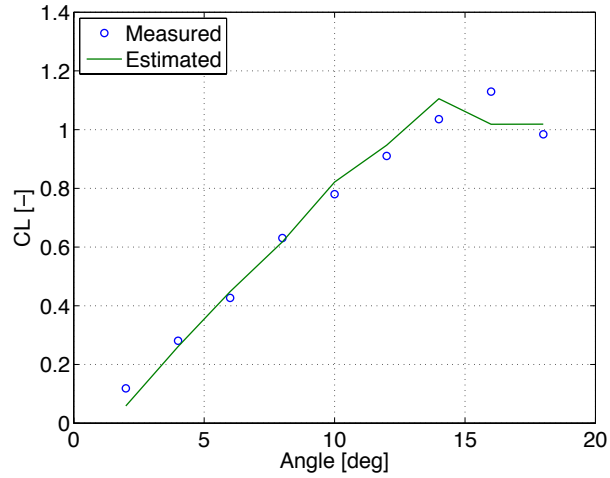

Figure 5: Steady flow lift coefficient estimation through stall using LESP

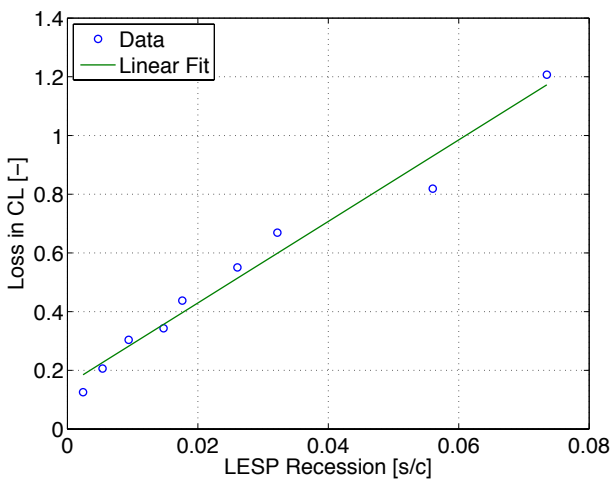

Figure 4: Steady flow Calibration of LESP recession with loss-in-lift coefficient

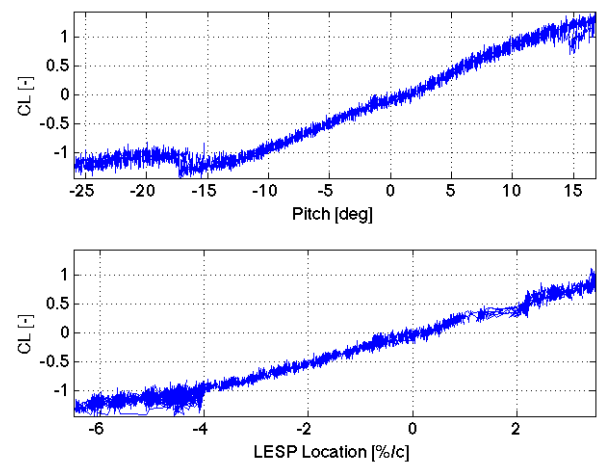

Figure 6: Steady-state lift coefficient versus LESP location and pitch angle

reasonably accurate.

To demonstrate the efficacy of using LESP versus a geometric measurement, e.g., pitch angle, Figure 6 depicts LESP versus lift coefficient as well as pitch angle versus lift coefficient during a pseudo-steady pitch sweep through the range of angles. The data shows that the pitch angle is nonlinear and non-monotonic with lift coefficient. Specifically, observe the behavior of the lift coefficient with pitch angle beyond stall, i.e., > 14 degrees. On the other hand, the LESP moves monotonically with lift coefficient, even through stall. Flow separation affects the aerodynamic forces and consequently affects the monotonicity of the lift versus pitch angle curve. With LESP, the effects of flow separation are effectively already considered, since LESP is related to the total circulation around the wing section. So, when the section circulation reduces, the LESP recedes towards the leading edge. Therefore, LESP is an ideal observable for feedback/feedforward control schemes in the presence of gust disturbances, because circulation changes are directly controlled resulting in a phase lead advantage over control schemes involving structural response.

In order to apply the phase lead of the LESP sensor, we must determine the effect of unsteadiness on the LESP output. Figure 7 depicts the response of the LESP sensor, pitch angle and plunge displacement sensors for the free PAPA wing undergoing LCO at 19 m/s. The lift coefficient versus LESP plot shows that there is a phase difference between the measured lift coefficient and the LESP output, and that the phase difference varies nonlinearly with pitch angle. There is a similar behavior with

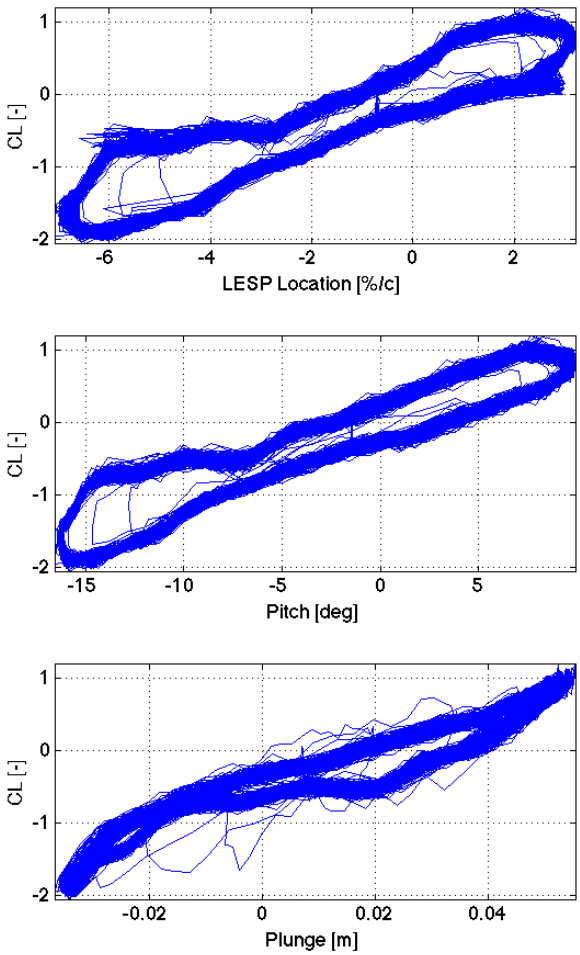

Figure 7: CL versus LESP, pitch angle and plunge displacement during an LCO

pitch angle. For the CL versus pitch angle plot, the phase difference is expected because of the second-order ODE relationship (with inertial, damping and stiffness terms) between pitch and plunge with aerodynamic forces and moments.

With respect to the relationship of LESP with CL, it is illustrative to break the unsteady lift into two parts: (1) circulatory lift and (2) non-circulatory lift. Non-circulatory lift is associated with the inertial term, i.e., added mass effects, and circulatory lift is associated with the bound vortex and wake. The LESP is directly correlated to the circulatory lift. Once the non-circulatory lift is estimated using pitch/plunge states and combined with the LESP measurements related to the circulatory lift, we obtain the total unsteady lift coefficient. The phase relationship between the aerodynamic forces and moments (as estimated using the LESP sensor and accelerometers) generated by the motion with the structural state provides a means to determine the stiffness and damping of the aeroservoelastic system, which relate directly to system stability.

Figure 8: Wing instrumented at three span stations

Figure 9: Instrumented wing in TAMU 3 ft $\times$ 4 ft tunnel

The second test is a forced PAPA test in which the wing is forced to undergo pitch as opposed to freely vibrating in the previous case. A wing with an airfoil section similar to that used in the X-56A vehicle is shown instrumented at 3 span stations with surface flow sensors in Figure 8. The objective of this test is to relate the movement of flow bifurcation points, e.g. LESP, and flow separation point to the aerodynamic forces under increasing pitch rates. This test will enable us to calibrate the wing for unsteady response, thereby providing a basis for flight testing the

actual MAD/MUTT wing with a model for the sensor dynamics.

Pitch/plunge tests have been conducted and are currently being analyzed. Once test results have been obtained, we will report the results along with the closed-loop free PAPA tests. These tests provide a sound basis for the further development and validation of the use of flow bifurcation points for control feedback on actual flight test vehicles. Results from this Seedling effort will be used to develop open-loop / closed-loop test procedures for upcoming tests on the F-18 with AFRL under the RASSCAL program, and follow-on NASA work in distributed aeroservoelastic control on the MUTT vehicle.

The free and forced PAPA at TAMU are providing valuable data and the ability to simulate closed-loop controllers to better understand aeroservoelasticity in the presence of nonlinearities in aerodynamics (flow separation), structures (nonlinear pitch stiffness) and actuation (freeplay). In particular, the forced PAPA data will be used for analytical and numerical computation fluid dynamics (CFD) validation.

Next Steps

Our next steps include the use of the forced PAPA facility to fully characterize the unsteady aerodynamics of the X-56A wing. Previously, we conducted wind tunnel tests on the forced and free pitch-and-plunge apparatus. The data from this test will be used for identifying an unsteady aerodynamic model.

The forced PAPA system has been implemented. The free PAPA system in the same wind tunnel is currently undergoing development and will be ready in time for our experimentation. We will be constructing a wing with relatively high bandwidth control surfaces (zero to 30 Hz) to enable demonstration of gust load alleviation.

The general data system shown in Figure 10 has been implemented for real-time use with the TAMU free and forced PAPA facility. For each data set, we record data from (1) accelerometers placed on the wing and PAPA, (2) 6-axis load balance for calculating the aerodynamic forces and moments from the total loads and moments, (3) pitch/plunge encoder positions, (4) control surface position, (5) the leading-edge stagnation point (LESP) location and (6) the static/dynamic pressure, i.e., P_s and q, and total temperature, T_t.

For example, Figure 11 depicts a sample data record for the onset of a limit cycle oscillation triggered by a control surface doublet. We can observe the unfiltered LESP signal (as movement in percentage chord) at the top, the normalized aerodynamic force in the lift direction, pitch

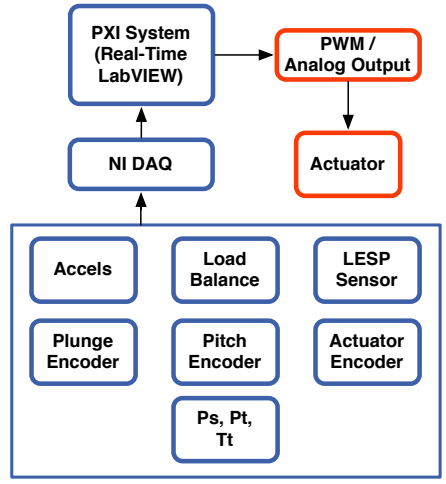

Figure 10: Real-Time system for data acquisition and deterministic control

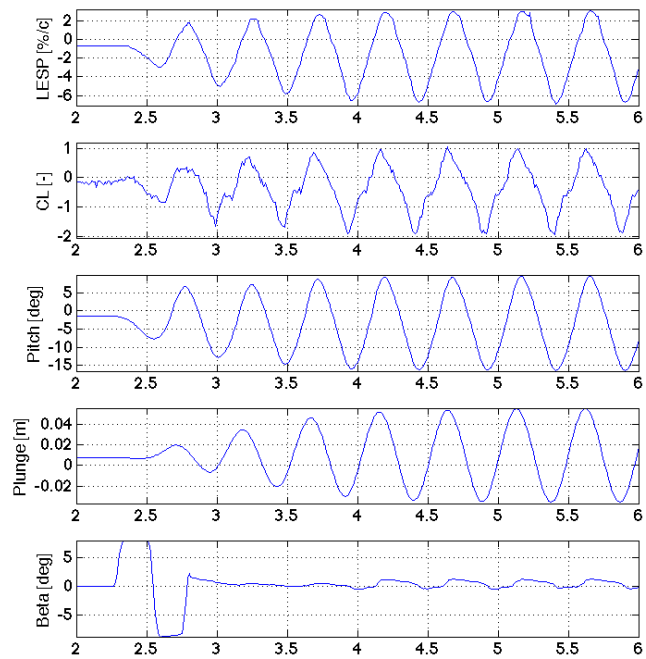

Figure 11: Beginning data record for limit cycle oscillation in the free PAPA

encoder position, plunge encoder position and finally the control surface deflection. The data was sampled at 500 Hz. The embedded PXI-based computer data system is capable of simultaneously recording and actuating the control surfaces. The control surfaces in this case were actuated at a frame rate of 50 Hz.

In our next steps, we will utilize the TAMU facilities to separate the effects of aerodynamics from elasticity. To

accomplish this separation, we first determine the unsteady aerodynamic model by (1) testing the wing in a forced pitch-and-plunge apparatus (PAPA), where we force the wing into predesignated pitch and plunge motion profiles, and (2) modeling the resulting unsteady aerodynamic forces and moments from the motion profile. Then utilizing the validated unsteady aerodynamic model, we test the same wing in the same facility but in a free PAPA. This enables the modeling/validation of the combined aeroservoelastic system. We can vary properties of the free PAPA to include/emulate nonlinearities, and change inertial/damping/stiffness properties. We further impose gust disturbances and model the complete system so that we could design/implement a control law that will achieve gust load alleviation under a range of parameter variations. The end result is a validated control law design that can be adapted to a flight platform, e.g., X-56A.

The pitch plunge drive system has an independent mechanism for each motion. Figure 13 shows an overall view of the mechanism, e.g., the wing in Fig. 13, is supported on both sides within two balances (load cells). The pitch motion is carried out by the pitch module which houses all the components responsible for pitch motion. The two pitch modules (one on each side of the section) are mounted on steel rails through linear bearings.

Figure 14 depicts the components of the pitch module. The wing is mounted to the balance via an interface plate which is responsible for determining the axis of rotation. The interface plate can be designed for any location of pitch axis between the LE and mid chord in the chordwise direction. The mean angle of attack (AOA) plate allows pitch oscillation about any AOA from 0 to 360 degrees at an interval of 5 degrees. At the end of the main wing shaft, an optical encoder measures the instantaneous angular position of the wing.

The oscillating motion is generated by the connecting rod. Figures 15 and 16 show pitch module and a close up of dummy wing-balance joint of the actual setup respectively.

The forced oscillation system will be used to generate custom gusts for the free vibration wing. Figure 12 shows the complete schematic of the free vibration wing in the wake of the gust generator. The free vibration wing is placed about 3 to 4 ft behind the gust generator wing. The wing assembly consists of the wing, a powered flap, two load balances (one on each side) and two struts (one on each side). The free pitch modules themselves are mounted on vertical rails and hence providing free plunge. The stiffness and non linearity of the pitch springs can be controlled by the mounting of springs. The plunge motion is constrained by plunge springs. The system can also be made free to plunge if the plunge stops are removed.

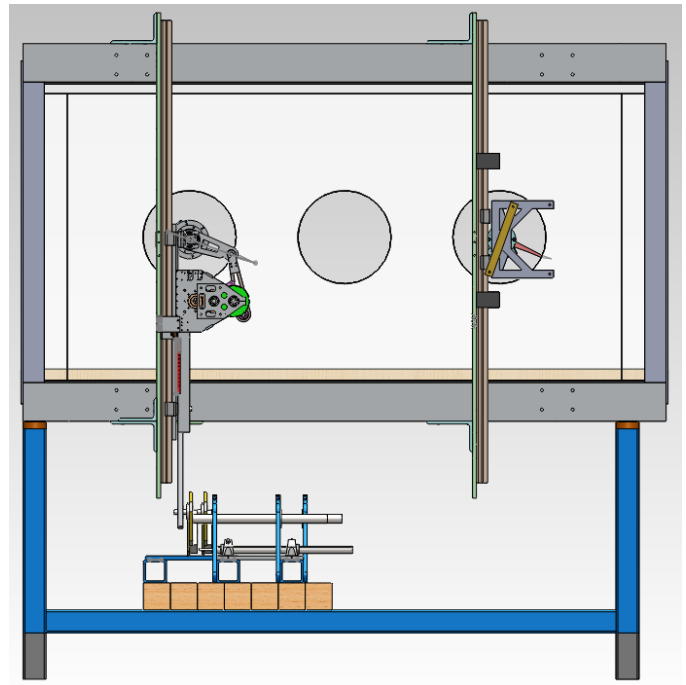

(a) Side View

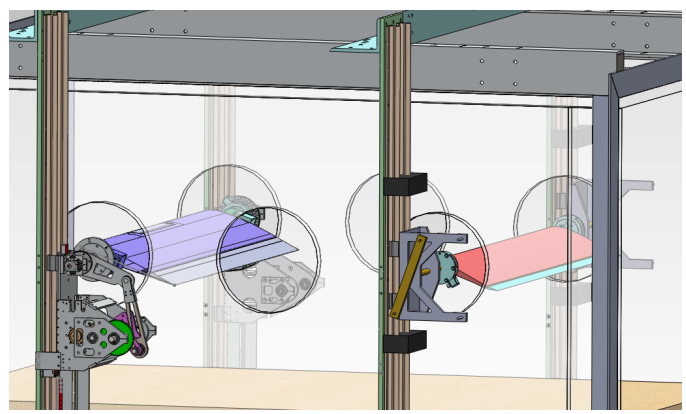

(b) Full View

Figure 12: Forced and free pitch and plunge apparatus (PAPA)

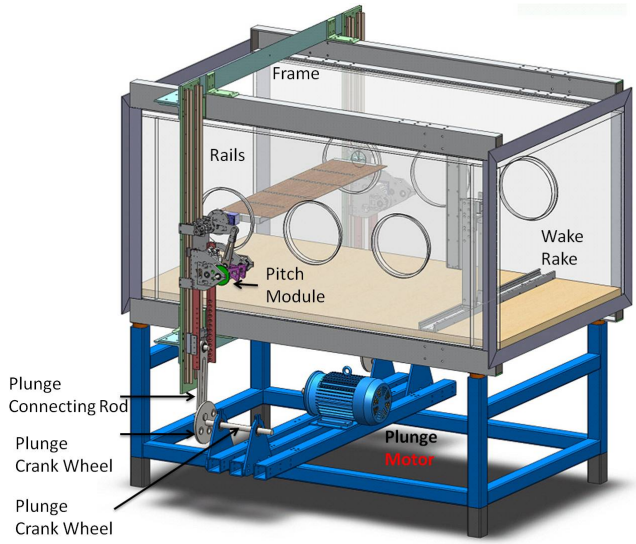

Figure 13: Pitch and plunge drive system

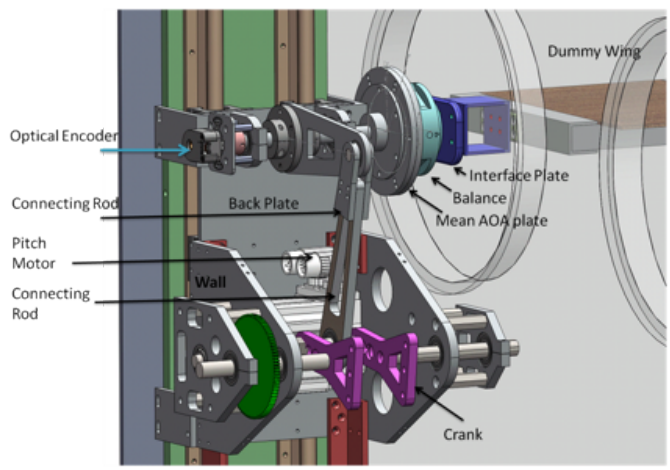

Figure 14: Close-up of the pitch module

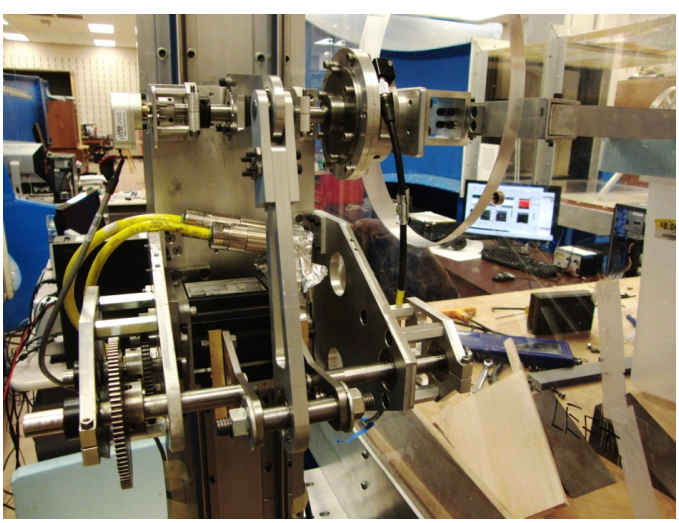

Figure 15: Pitch module: actual setup

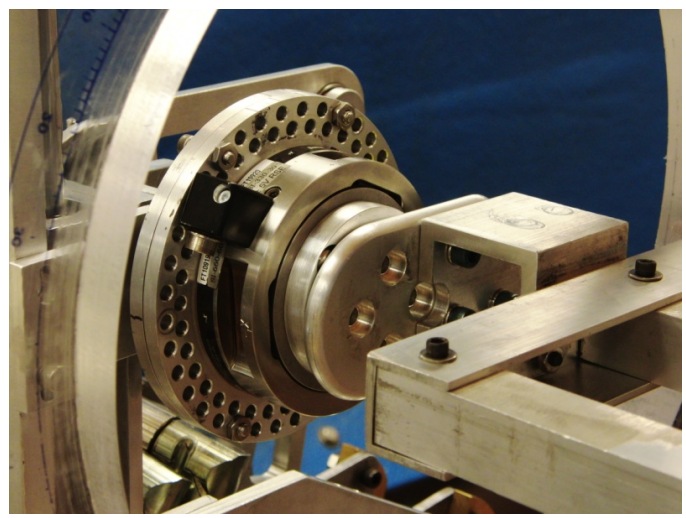

Figure 16: Close-up of the wing-load balance interface

Current TRL: 4

Applicable NASA Programs/Projects

[ARMD] Instrumentation / measurement technology / test technique for aeronautics in all flight regimes, Distributed and autonomous concept for aviation and extra-terrestrial vehicles, Technology enabling new flight applications with aeroelastic sensor networks, Game-changing flight vehicle concept for performance enhancement.

[FAP] Reduce drag & weight; Increase performance & energy efficiency; Improve computational / experimental tools & processes with reduced uncertainty; Develop, test, analyze advanced multi-disciplinary concepts/technologies.

[SFW] Expressed interest and support for this research in FY12-16 for LAPS. [SUP] Supporting flight testing on the MUTT and F-18 FAST aircraft to investigate subsonic-to-supersonic shock formation and shock-boundary layer interaction besides LESP for control.

[AvSP] Loss-of-control prevention / mitigation / recovery in hazardous flight conditions.

[NASA OCT-CIF] NASAs Office of Chief Technologist / Center Innovation Fund has also expressed interest in this research as an ARMD-external partner and contributed substantially to the effort with supplemental funding.

[External] LMCO for flight test applications and follow-on R&D for MAD; AFRL procurement funding for R&D under the RASSCAL program; and Texas A&M and University of Minnesota for testing support, distributed controls and aerostructures modeling research for controls.

Publications and Patent Applications

A NASA report and AIAA conference paper are in progress to summarize the Phase 1 work.